REPORT DOCUMENTATION PAGE

Form Approved
OMB No. 0704-0188

PLEASE DO NOT RETURN YOUR FORM TO THE ABOVE ORGANIZATION.

1. REPORT DATE *(DD-MM-YYYY)*	2. REPORT TYPE	3. DATES COVERED *(From - To)*
11-04-2014	Journal Article	

4. TITLE AND SUBTITLE

Wavelet analysis of near-inertial currents at the East Flower Garden Bank

5a. CONTRACT NUMBER

5b. GRANT NUMBER

5c. PROGRAM ELEMENT NUMBER

0602435N

6. AUTHOR(S)

W.J. Teague, H.W. Wijesekera, E. Jarosz, A. Lugo-Fernández, Z.R. Hallock

5d. PROJECT NUMBER

5e. TASK NUMBER

5f. WORK UNIT NUMBER

73-4876-03-5

7. PERFORMING ORGANIZATION NAME(S) AND ADDRESS(ES)

Naval Research Laboratory
Oceanography Division
Stennis Space Center, MS 39529-5004

8. PERFORMING ORGANIZATION REPORT NUMBER

NRL/JA/7330--14-2114

9. SPONSORING/MONITORING AGENCY NAME(S) AND ADDRESS(ES)

Office of Naval Research
One Liberty Center
875 North Randolph Street, Suite 1425
Arlington, VA 22203-1995

10. SPONSOR/MONITOR'S ACRONYM(S)

ONR

11. SPONSOR/MONITOR'S REPORT NUMBER(S)

12. DISTRIBUTION/AVAILABILITY STATEMENT

Approved for public release, distribution is unlimited.

13. SUPPLEMENTARY NOTES

14. ABSTRACT

Near-inertial currents (NICs) often dominate the mean circulation at the East Flower Garden Bank (EFGB), part of the Flower Garden Banks National Marine Sanctuary. The EFGB, one of several submerged coral reefs, is located in the northwestern Gulf of Mexico, about 190 km southeast of Galveston, Texas. The bank is about 6 km wide in the east -west direction and rises to within about 20 m from the surface. NICs near the EFGB are described using current data from 5 acoustic Doppler current profilers that were moored at the edges of the bank and on top of the bank for about a year. A wavelet analysis was used in order to better describe the nonstationarity of the NICs. NICs were strongest during spring and summer due to their near resonant response with sea breeze and the shallowness of the mixed layer, and exhibited a first-baroclinic-mode vertical structure. NICS were generally larger near the surface and extended to the bottom on the west side of the EFGB but only to within about 20 m of the bottom on the eastern side of the bank. NIC ellipses were nearly circular and rotated clockwise above the top of the EFGB but became flatter and aligned with the bathymetry with increasing depth; occasionally, on the eastern side of the bank, the NIC vectors rotated counterclockwise due to probable effects of lee vortices arising from the mean flow interacting with the bank. Most energy input by the wind at the surface was likely transferred downward through divergence of the meridional flow against the coastal boundary. The inertial currents were at times more energetic than the mean flow, and often accounted for more than 50% of the total current energy.

15. SUBJECT TERMS

East Flower Garden Bank; Currents; Inertial Oscillations; Temperature/salinity; ADCP; Northwestern Gulf of Mexico (27–28N, 93–94W)

16. SECURITY CLASSIFICATION OF:			17. LIMITATION OF ABSTRACT	18. NUMBER OF PAGES	19a. NAME OF RESPONSIBLE PERSON
a. REPORT	b. ABSTRACT	c. THIS PAGE			William J. Teague
Unclassified	Unclassified	Unclassified	UU	14	19b. TELEPHONE NUMBER *(Include area code)* (228) 688-4734

Reset

Standard Form 298 (Rev. 8/98)
Prescribed by ANSI Std. Z39.18

PUBLICATION OR PRESENTATION RELEASE REQUEST 14-1231-0919

Pubkey: 9172 NRLINST 5600.2

Ref: (a) NRL Instruction 5600.2
(b) NRL Instruction 5510.40D

Encl: (1) Two copies of subject paper (or abstract)

( ) Abstract only, published	( ) Abstract only, not published
( ) Book	( ) Book chapter
( ) Conference Proceedings (refereed)	( ) Conference Proceedings (not refereed)
( ) Invited speaker	( ) Multimedia report
(X) Journal article (refereed)	( ) Journal article (not refereed)
( ) Oral Presentation, published	( ) Oral Presentation, not published
( ) Other, explain	

STRN NRL/JA/7330-14-2114
Route Sheet No. 7330/
Job Order No. 73-4876-03-5
Classification X U C
Sponsor ONR B. 6.1
approval obtained ___ yes X no

Title of Paper or Presentation
Wavelet Analysis of Near-Inertial Currents at the East Flower Garden Bank

Author(s) Name(s) *(First,MI,Last), Code, Affiliation if not NRL*

William J. Teague 7332 **Hemantha W Wijesekera** 7332 **Ewa Jarosz** 7332 **A. Lugo-Fernandez** Bureau of Ocean Energy Mgmt. - N.O., LA
Z.R. Hallock NVision Solutions

It is intended to offer this paper to the _____
(Name of Conference)

(Date, Place and Classification of Conference)

and/or for publication in **Continental Shelf Research, Unclassified** _____
(Name and Classification of Publication) *(Name of Publisher)*

After presentation or publication, pertinent publication/presentation data will be entered in the publications data base, in accordance with reference (a).
It is the opinion of the author that the subject paper (is ____) (is not X) classified, in accordance with reference (b).
This paper does not violate any disclosure of trade secrets or suggestions of outside individuals or concerns which have been communicated to the Laboratory in confidence. This paper (does ____) (does not X) contain any militarily critical technology.
This subject paper (has ____) (has never X) been incorporated in an official NRL Report.

William J. Teague, 7332 _____
Name and Code *(Principal Author)* (Signature)

CODE	SIGNATURE	DATE	COMMENTS
Author(s) Teague	W J Teague	3/19/14	Need by 10 Apr 14
			Publicly accessible sources used for this publication
			This is a Final Security Review. Any changes made in the document, after approved by Code 1231, nullify the Security Review.
Section Head Teague	W J Teague	3/19/14	
Branch Head Richard L. Crout, 7330	R L Crout	3-19-2014	
Division Head Ruth H. Preller, 7300	R H Preller	3/19/14	1. Release of this paper is approved. 2. To the best knowledge of this Division, the subject matter of this paper (has ____) (has never X) been classified.
Security, Code 1231	M Lisa	3/20/14	1. Paper or abstract was released. 2. A copy is filed in this office.
Office of Counsel,Code 1008.3	Kathy Chapman	4-9-14	
ADOR/Director NCST E. R. Franchi, 7000			
Public Affairs *(Unclassified/ Unlimited Only)*, Code 7030.4	Shannon Mennis	4-9-14	
Division, Code			
Author, Code			

20 MAR '14 PM 3:58

HQ-NRL 5511/6 (Rev. 12-98) (e) THIS FORM CANCELS AND SUPERSEDES ALL PREVIOUS VERSIONS

Continental Shelf Research 88 (2014) 47–60

Contents lists available at ScienceDirect

Continental Shelf Research

journal homepage: www.elsevier.com/locate/csr

Research papers

Wavelet analysis of near-inertial currents at the East Flower Garden Bank

W.J. Teague [a,*], H.W. Wijesekera [a], E. Jarosz [a], A. Lugo-Fernández [b], Z.R. Hallock [c]

[a] Naval Research Laboratory, Stennis Space Center, MS 39529, USA
[b] Bureau of Ocean Energy Management, New Orleans, LA 70123, USA
[c] NVision Solutions, Inc., Bay St. Louis, MS 39520, USA

ARTICLE INFO

Article history:
Received 2 April 2014
Received in revised form
26 June 2014
Accepted 30 June 2014
Available online 11 July 2014

Keywords:
East Flower Garden Bank
Currents
Inertial Oscillations
Temperature/salinity
ADCP
Northwestern Gulf of Mexico (27–28N, 93–94W)

ABSTRACT

Near-inertial currents (NICs) often dominate the mean circulation at the East Flower Garden Bank (EFGB), part of the Flower Garden Banks National Marine Sanctuary. The EFGB, one of several submerged coral reefs, is located in the northwestern Gulf of Mexico, about 190 km southeast of Galveston, Texas. The bank is about 6 km wide in the east–west direction and rises to within about 20 m from the surface. NICs near the EFGB are described using current data from 5 acoustic Doppler current profilers that were moored at the edges of the bank and on top of the bank for about a year. A wavelet analysis was used in order to better describe the nonstationarity of the NICs. NICs were strongest during spring and summer due to their near resonant response with sea breeze and the shallowness of the mixed layer, and exhibited a first-baroclinic-mode vertical structure. NICS were generally larger near the surface and extended to the bottom on the west side of the EFGB but only to within about 20 m of the bottom on the eastern side of the bank. NIC ellipses were nearly circular and rotated clockwise above the top of the EFGB but became flatter and aligned with the bathymetry with increasing depth; occasionally, on the eastern side of the bank, the NIC vectors rotated counterclockwise due to probable effects of lee vortices arising from the mean flow interacting with the bank. Most energy input by the wind at the surface was likely transferred downward through divergence of the meridional flow against the coastal boundary. The inertial currents were at times more energetic than the mean flow, and often accounted for more than 50% of the total current energy.

Published by Elsevier Ltd.

1. Introduction

Near-inertial current (NIC) oscillations are common to the open ocean and to shelf regions (Webster, 1968). They are ubiquitous on the shelf in the northern Gulf of Mexico (Chen et al., 1996; DiMarco et al., 2000). NICs are characterized by clockwise (in the northern hemisphere) rotations of nearly circular horizontal currents at frequencies at or near the local inertial frequency (Pollard, 1970; Perkins, 1972; Kundu, 1976). NICs are forced by winds and most effectively by wind pulses on time scales of less than half of the local inertial period (Pollard, 1970; Perkins, 1972). Existing NICs can be enhanced by diurnal sea-breeze forcing if the currents and sea breeze are in phase (near-resonant conditions near 30° latitude) (Simpson et al., 2002; DiMarco et al., 2000; Jarosz et al., 2007). Inertial oscillations have been observed after the passage of hurricanes (Price, 1976; Brooks, 1983, Teague et al., 2007) and atmospheric cold fronts (Chen et al., 1996; Halper et al., 1988; Daddido et al., 1978). They can last from several days when generated by local winds and cold fronts to more than a week when generated by storms and hurricanes. NICs can generate the largest percentage of current variance, particularly where tides are weak, for periods of about a day. They commonly are of the order of magnitude of tidal variance in the northern Gulf of Mexico (Chen et al., 1996).

Long-term measurements of current velocity, temperature, and salinity were made at the East Flower Garden Bank (EFGB) from December 2010 to December 2011 (Fig. 1a). The EFGB is part of a marine sanctuary designated as the Flower Garden Banks National Marine Sanctuary, and is managed by the National Oceanic and Atmospheric Administration (NOAA). The Flower Gardens, the northern-most live coral reef in the Gulf of Mexico, are located near the edge of the Texas–Louisiana continental shelf in the northwestern Gulf of Mexico (see http://flowergarden.noaa.gov). The EFGB is about 6 km wide in the along-shelf direction and 10 km in length, and peaks at about 20 m below the surface. The EFGB is quite steep on the eastern and southern sides and less so on the western and northern sides. All of the banks are surrounded by oil and gas activities. Interactions of the bank with the

* Corresponding author. Tel.: +1 228 688 4734.
E-mail address: William.Teague@nrlssc.navy.mil (W.J. Teague).

http://dx.doi.org/10.1016/j.csr.2014.06.013
0278-4343/Published by Elsevier Ltd.

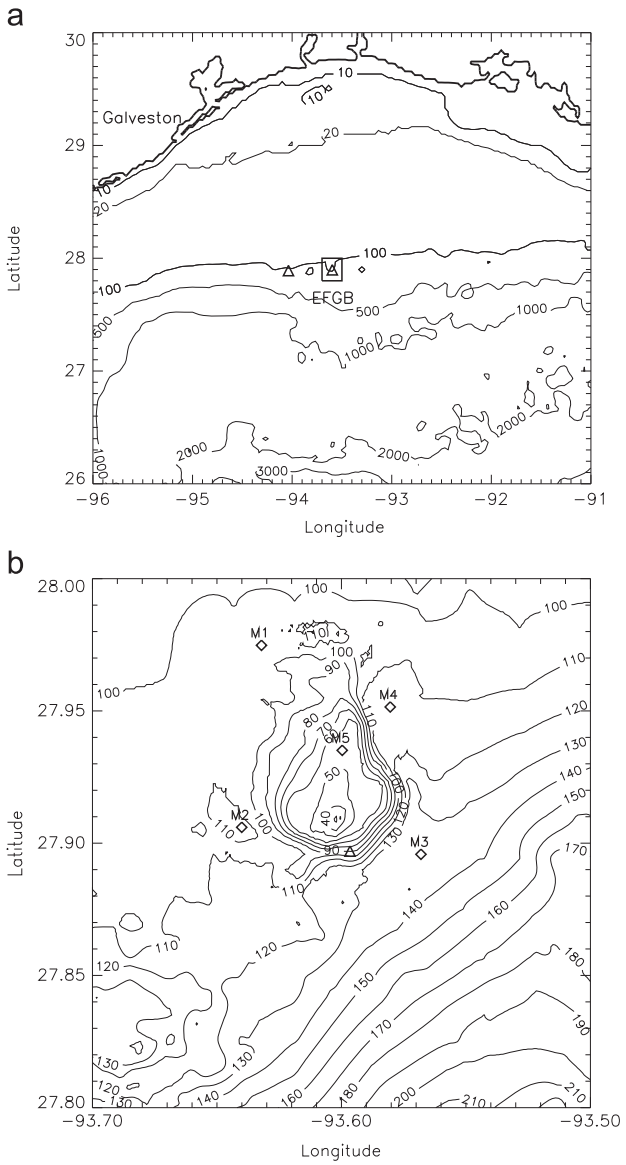

Fig. 1. (a) Experiment area off the Texas–Louisiana coast indicated by the box near the shelf edge (100 m isobath). Triangles denote positions of meteorological stations. (b) Locations of ADCP moorings (M1–M5) at the East Flower Garden Bank (EFGB) located near the shelf break in the northwestern Gulf of Mexico. Bathymetry contours are every 10 m. Temperature/salinity strings S1–S4 (not shown) were within about 200 m of corresponding M1–M4 ADCPs. The triangle denotes the position of the easternmost meteorological station.

currents are important in processes over the bank. Protecting this natural habitat is very important to the ecology of the entire Gulf of Mexico. NICs are usually generated at the surface by the local winds, but circulation over rough bathymetric features at the edge of the shelf, such as the EFGB, may impact the structure and dynamics of the NICs and ultimately influence submesoscale mixing processes (Moum and Nash, 2000) at this bank, which may impact other nearby banks as well. The NICs can also contribute significantly to the overall current variability at the EFGB.

The objective of this work is to characterize the impact of a submerged bank near the shelf edge on the current flow which is important for understanding of mixing and exchange mechanisms between the deep ocean and the shelf, and to describe the structure of near inertial currents over depth and time at locations surrounding and on top of EFGB under various wind forcing conditions. The effects of banks on inertial oscillations in modifying their structure and dynamics are not now well understood due to a scarcity of current measurements next to submerged banks. The structure of inertial oscillations at the EFGB has never been studied. The EFGB is large enough to alter the circulation at the shelf edge (Teague et al., 2013) and hence should have an effect on the inertial oscillations. The NICs can reverse the usual eastward mean flow over the bank when their amplitudes become large but these reversals may just last a few hours (Teague et al., 2013). NICs can impact the dispersion of contaminants, biological organisms, and inorganic materials and hence may play a key role in bank habitats and oceanography.

The remainder of the paper is organized as follows. Current data are described in Section 2, and wind and pressure data are described in Section 3. The methodology for calculation of the mixed-layer depth and a brief description of the mixed layers are provided in Section 4. The wavelet analysis of the currents is described in Section 5. Similarly, a wavelet analysis is applied to the winds in Section 6. Results for the diurnal–inertial band, based on the wavelet analysis, of the currents are presented in section 7. Finally, some discussion and conclusions are given in Sections 8 and 9, respectively.

2. Current data

Four acoustic Doppler current profilers (ADCPs, M1–M4) were moored on the bottom at the edge and one ADCP (M5) was moored near the top of the EFGB from December 2010 to December 2011. All moorings were recovered and redeployed in June 2011. Locations of the moorings and bathymetry are shown in Fig. 1b. M5 was located just to the north of the peak of the bank, at a depth of 47 m. M1–M4 were deployed just NW, SW, SE and NE, respectively, of the EFGB, at depths ranging from 100 to 127 m.

RD Instruments Workhorse ADCPs, operating at 300 kH (M1–M4) and 600 kHz (M5), were mounted in trawl-resistant pods that rested on the bottom and are referred to as Barnys due to their barnacle-like shape (Perkins et al., 2000). They recorded nearly full water column current profiles at 2 m vertical resolution except for 4 m vertical resolution at M3 every 12 or 15 min. ADCP accuracy is 0.5% of the water velocity. The usual naming conventions for the velocities are used: U positive towards the east, V positive towards the north, and W positive upwards. Further details on the data can be found in Teague et al. (2013). After initial processing and editing, ADCP data were resampled at even 30-min times (compatible with wind data), and time-trimmed (at the series ends) so that all series from deployment 1 (D1) started and stopped at the same times (except for M5 which was short), and similarly for deployment 2 (D2).

Above the EFGB (shallower than about 40 m) horizontal velocities are significantly correlated. EOF analyses applied to U and V at 20 m and 40 m depths show that more than 80% of overall variance was in the first horizontal EOF mode and less than 10% in mode 2 at 20 m. The mode 1 amplitudes are virtually constant for all moorings used (M1–M4 in deployment 1, M1–M5 in deployment 2), and mode 1 explained variance for each location is at least 75% at 20 m. Overall first-mode variance decreases with depth with an explained variance minimum of 60% at 40 m. This result implies that on the relatively-small horizontal extent of the observations that currents above the depth of the EFGB are laterally highly coherent and in phase.

Inertial periods at the center, northern, and southern edges of the EFGB, using the 100 m isobath as the boundary, are approximately 25.55 h, 25.52 h, and 25.58 h, respectively. The 3 major tidal components are M2, K1, and O1 and have periods of 12.42 h, 23.93 h, and 25.82 h, respectively. The ADCP data were harmonically analyzed for 4 diurnal and 4 semidiurnal tidal constituents (K_1, O_1, P_1, Q_1, N_2, M_2, S_2, K_2). This analysis was done using depth-

averaged currents at M1–M4; D1 and D2 records were concatenated yielding overall record lengths of nearly one year (363.8 days). The M5 records were excluded since M5-D1 was only 40 days long. The Rayleigh criteria for most combinations of the selected constituents are about 27 days or less; for K_1 and P_1, as well as for K_2 and S_2, it is 182.6, well below the record length of 363 days; however, the year-long record is necessary for K_2 due to possible aliasing with a semiannual constituent. There were small variations of amplitudes among the mooring sites which may be due to shoaling effects near the shelf edge and the bank. The amplitudes for O_1, K_1 and M_2 were approximately 1.9 cm s^{-1}, 2.3 cm s^{-1} and 2.2 cm s^{-1}, respectively. The other 5 constituent amplitudes were small (<1 cm s^{-1}). These amplitudes are somewhat smaller than those reported by DiMarco and Reid, (1998). Amplitudes of the inertial oscillations can exceed 15 cm s^{-1} and are often larger than tidal amplitudes. NICs can be modified by the diurnal tide, depending on the phase difference, but this effect is relatively small. Rotary autospectra for current velocity at 7.5 m depth from M1 are displayed in Fig. 2 and show a strong clockwise (CW) peak near the diurnal–inertial as well as semidiurnal periods. There is little energy at the diurnal frequency for the counterclockwise (CCW) component but some CCW semi-diurnal energy is present but at a lower level than for the CW component. Removal of principal barotropic tidal constituents (also Fig. 2) attenuates much of the semidiurnal energy but the CW diurnal–inertial peak is minimally affected.

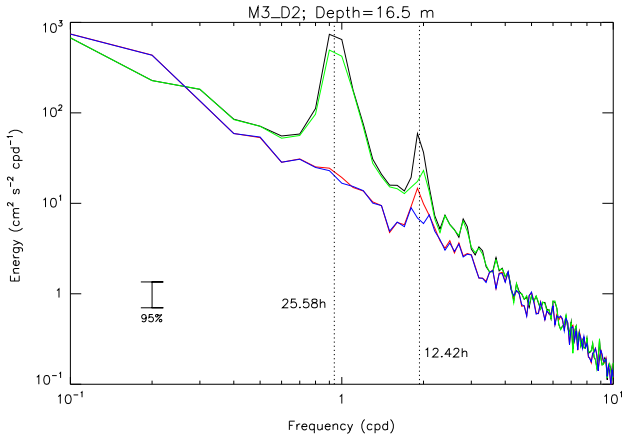

Fig. 2. Rotary autospectra for ADCP M3–D2. CW: with tides (black); barotropic tides removed (green). CCW: with tides (red); barotropic tides removed (blue). (For interpretation of the references to color in this figure legend, the reader is referred to the web version of this article.)

Overall average squared vertical shear of horizontal currents ($Sh^2=(\partial U/\partial z)^2+(\partial V/\partial z)^2$) ranged from 0.005 s^{-2} to 0.011 s^{-2} at mooring sites. The squared shear combined with vertical density gradients (based on temperature and salinity data from string moorings, Section 4) were used to calculate gradient Richardson numbers, $R_i=N^2/Sh^2$, where N^2 is the buoyancy frequency. With a few exceptions, some of which were likely spurious, R_i values were above 0.25 indicating vertical stability over most of the record. R_i values in the mixed layer were not included since both vertical shear and density gradients were small.

3. Wind and pressure data

Wind velocity and atmospheric pressure data were collected half-hourly at the southern edge of the EFGB at National Data Buoy Center Station 42047, and at Station 42046 located approximately 37 km west of the EFGB. Winds were very similar between these two stations for the concurrent recording periods. Winds at 42046 were used when 42047 was out of service which was about half of the year-long mooring period. Winds during the deployment period were typical for this region (de Velasco and Winant, 1996). Wind velocities and pressures are shown in Fig. 3. Wind gusts are considerably larger than the 30-min averaged velocities. The atmospheric pressure record shows numerous frontal passages from December 2010 to May (days −30 to 130) and from October 2011 through December 2011 (days 270–360). Winds were weakest mainly during summer (except for a wind event near day 245), and were generally southerly. Hurricanes or tropical storms did not impact the EFGB in 2011 and atmospheric pressure was almost always above 1000 mb (Fig. 3). There is a significant peak in the clockwise (CW) rotary wind autospectrum (Fig. 4) for the summer period that may be associated with sea-breeze effects (Zhang et al., 2009). The most intense inertial oscillations were found during spring and summer. These enhanced amplitudes are associated with a near-resonant response to sea-breeze effects (Teague et al., 2013; Zhang et al., 2009; Jarosz et al., 2007; Simpson et al., 2002; DiMarco et al., 2000). The EFGB is about 200 km off the Texas–Louisiana coastline and is considerably farther offshore

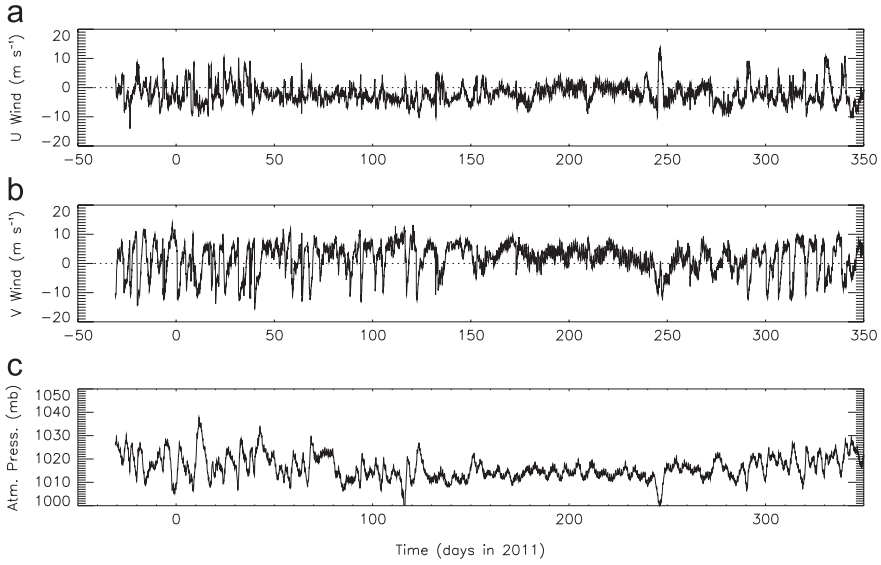

Fig. 3. Eastward (a) and northward (b) components of wind velocity; atmospheric pressure (c), near the EFGB. First sample on 1 December 2010.

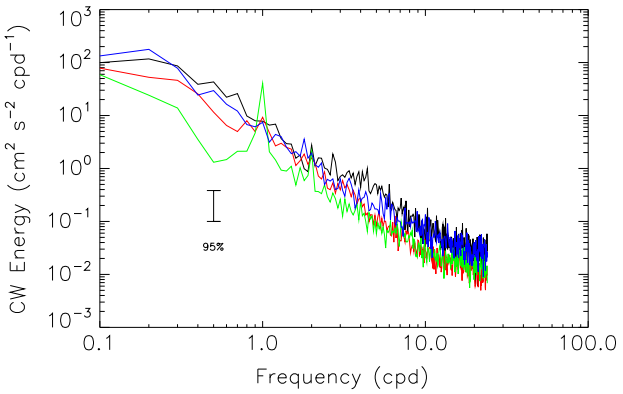

Fig. 4. Clockwise (CW) rotary autospectra of the wind velocity for each season (black-winter, red-spring, summer-green, fall-blue) are shown. A significant diurnal peak is present for the summer (July–September). CCW spectra (not shown) are similar, but a diurnal peak is not present. (For interpretation of the references to color in this figure legend, the reader is referred to the web version of this article.)

than the 50 km range that Chen et al. (1996) suggested that sea-breeze effects could be significant. However, Zhang et al. (2009) found that the sea breeze can extend to 300 km off the coast in this region.

4. Mixed-layer depths

Temperature data from string moorings located near (within several hundred meters) M1–M4 were used to estimate the mixed-layer depth (MLD) (Teague et al., 2013). Temperature from string mooring instruments (typically 10) were interpolated to one-meter intervals, but not extrapolated to the surface. The MLD was defined as the depth where the temperature changed by at least 0.25 °C from the shallowest temperature measurement. The MLDs computed from each string were smoothed over 24 h to reduce the higher frequency variability. Finally, the average MLD over all the strings was computed and a five-day boxcar average was applied to reduce the daily variability. MLDs were deepest, 60–80 m, during December and January. Throughout much of the year, MLDS ranged between 20 and 40 m. Rapid changes in the MLD may have been caused by eddy passages, such as the rapid decrease in MLD during March (Teague et al., 2013). The seasonal cycle in MLD at the EFGB is similar to that reported by McGrail (1983). The average MLD is shown in the upcoming wavelet plots (Figs. 12–19).

5. Wavelet analysis

Currents at the EFGB change quickly over time due to passing eddies, rapidly changing wind fields, and interaction with the bank. Hence the current patterns are not very predictable (Teague et al., 2013). These currents are not stationary and conventional Fourier spectrum analysis, which provides information about the average amplitude and phase for each harmonic and energy content for the entire time span of the data, presumes the data are stationary. This method, however, does not provide information about the energy levels and its variations within the time span of the data records. Wavelet analyses of ocean currents (Liu and Miller, 1996) can provide an effective way of obtaining time–frequency information of non-stationary processes such as NICs. Wavelet analysis provides a complementary approach to the traditional Fourier spectrum analysis, and is used here to provide a description of the time evolution of NICs near the EFGB. Significant current fluctuation energy is present in the ADCP velocity series acquired near the EFGB. The objectives here are to show the importance of variability in the diurnal–inertial band (DIB) relative to fluctuations at other frequencies, to describe the characteristics of variability in the DIB, to examine the relationship of DIB variability with local hydrographic conditions, and to calculate coherences between currents and wind velocity over the area.

Wavelet decomposition of a time series is essentially the systematic application of a set of band-pass filters whose bandwidths are proportional to the center periods of each (Torrence and Compo, 1998; Mallat, 1989). Here, we apply continuous wavelet transforms (CWTs) using a complex Morlet wavelet, with MATLAB software developed by Torrence and Compo (1998). The complex Morlet wavelet is essentially a cosine, sine wave with a Gaussian envelope for the real, imaginary parts, respectively; these functions are then convolved with the data to produce a set of band-passed complex series for each variable where the imaginary part is shifted by -90° from the real part. Wavelet decomposition was done with the half-hourly-sampled current series, and with the local wind data.

The wavelet analysis results in complex series of U and V velocity components which are functions of depth, time and frequency band, e.g.

$$U(z,t)=\sum_k \tilde{U}(z,t,f_k)=\sum_k \left(\tilde{U}_r(z,t,f_k)+i\tilde{U}_i(z,t,f_k)\right), \quad (1)$$

where the tilde indicates wavelet decomposition and k corresponds to a particular band. Following Gonella (1972), and Mooers (1973) band-limited velocities can be transformed to rotary components

$$\begin{aligned} 2\tilde{U}^+ &= \tilde{U}_r-\tilde{V}_i,\\ 2V^+ &= \tilde{U}_i+\tilde{V}_r,\\ 2\tilde{U}^- &= \tilde{U}_r+\tilde{V}_i,\\ 2\tilde{V}^- &= \tilde{U}_i-\tilde{V}_r, \end{aligned} \quad (2)$$

where the plus and minus superscripts indicate CCW and CW rotation, respectively, of the velocity vector. We calculate specific energy

$$\tilde{S}=\left|\tilde{U}\right|^2+\left|\tilde{V}\right|^2, \quad (3)$$

for total velocity; energies for CCW and CW currents, $\tilde{S}^+$ and $\tilde{S}^-$, are similarly defined. Plots of $\tilde{S}^-$ and $\tilde{S}^+$ for depths of 20 m (M1–M5), 40 m (for M5) and 70 m (M1–M4) appear as Figs. 5–8. The y-axis shows the period instead of the frequency for easier visualization. The inertial oscillations will appear in the CW spectra at periods just greater than a day for the latitude of the EFGB. Because the inertial oscillations rotate clockwise, they are not evident in the CCW spectra in the Northern Hemisphere.

The most prominent features in Fig. 5 ($\sim$20 m) are the bursts of CW DIB energy, strongest between days 100 and 250, at all mooring locations. This should not be surprising given the diurnal peak, associated with the sea breeze, in the CW wind spectrum (Fig. 4) during this time period. The high CW energy near the inertial period at day 245 is associated with a large north-northwesterly wind burst (Fig. 3). Some bursts of semi-diurnal energy are also evident, especially near day 170 but, as indicated above, much of this may be tidal. Lower-frequency (LF) energy is also present, but is generally lower than that in the DIB. In particular, there are several bursts at periods of several days near times 250, 260 and 320 days. Also, between days 220 and 280 there is a persistent burst of $\sim$17-day-period energy, primarily at M2, M3 and M5. DIB energy is essentially absent in plots of CCW energy (Fig. 6). The LF features, on the other hand, are more pronounced and also show up prominently at all mooring locations, with quite similar signatures, between days 230 and 280. LF CCW features also appear near days 40–50, primarily at M2 and

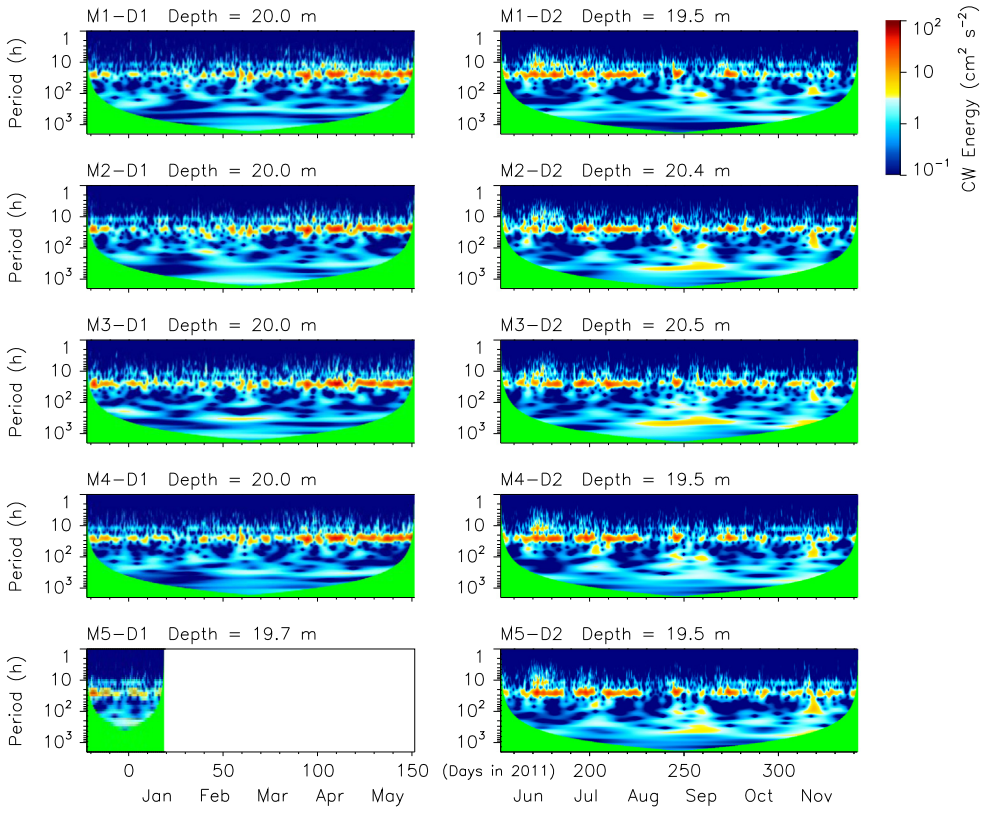

Fig. 5. Clockwise (CW) energy for currents near depth=20 m, as functions of period and time. Green areas indicate truncation limits, most evident for longer periods. (For interpretation of the references to color in this figure legend, the reader is referred to the web version of this article.)

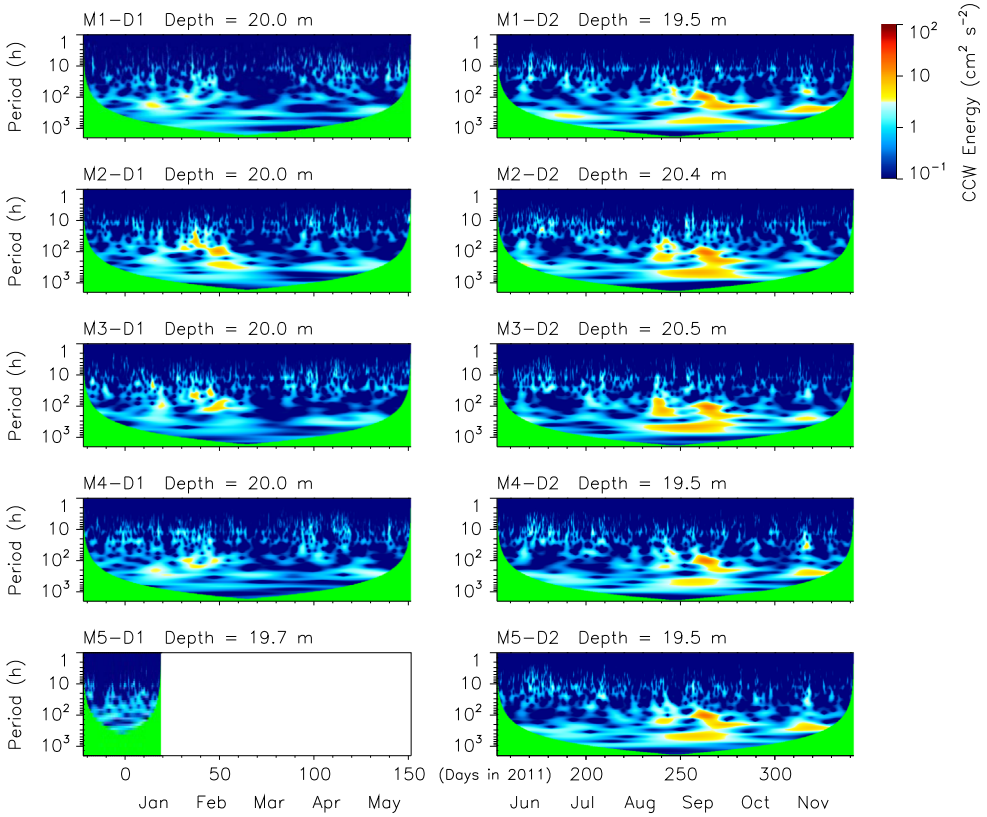

Fig. 6. Counterclockwise (CCW) energy for currents near depth=20 m, as functions of period and time. Green areas indicate truncation limits, most evident for longer periods. (For interpretation of the references to color in this figure legend, the reader is referred to the web version of this article.)

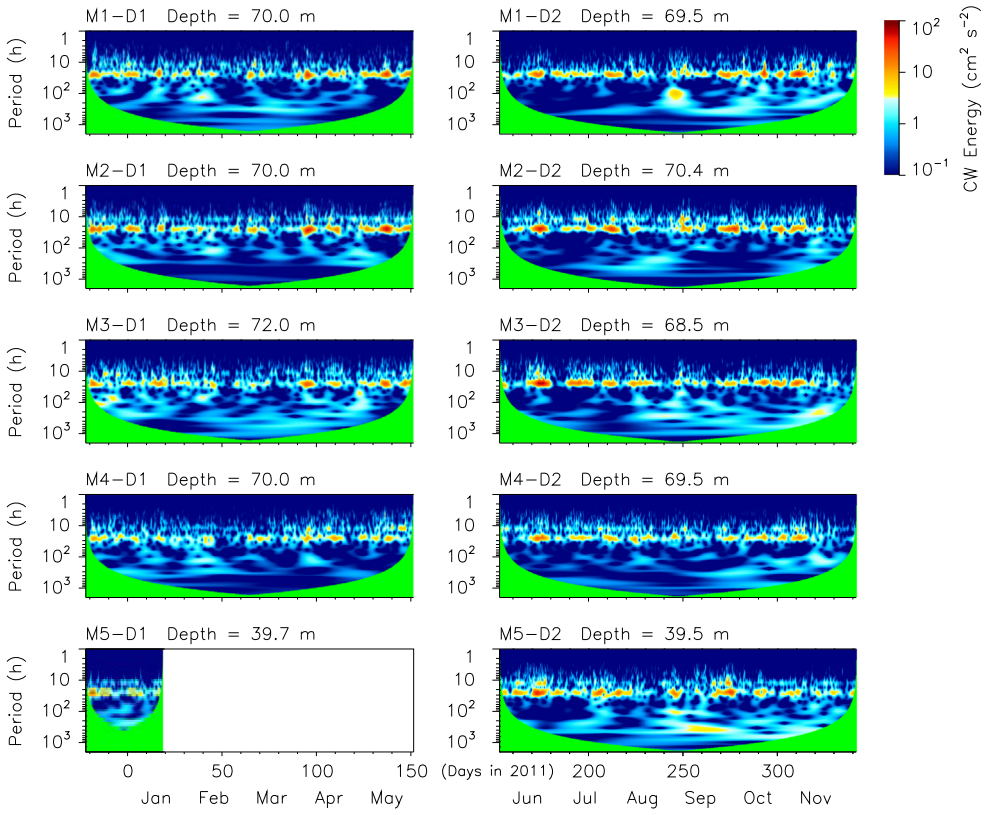

Fig. 7. Clockwise (CW) energy for currents near depth=70 m (M1–M4) and 40 m (M5), as functions of period and time. Green areas indicate truncation limits, most evident for longer periods. (For interpretation of the references to color in this figure legend, the reader is referred to the web version of this article.)

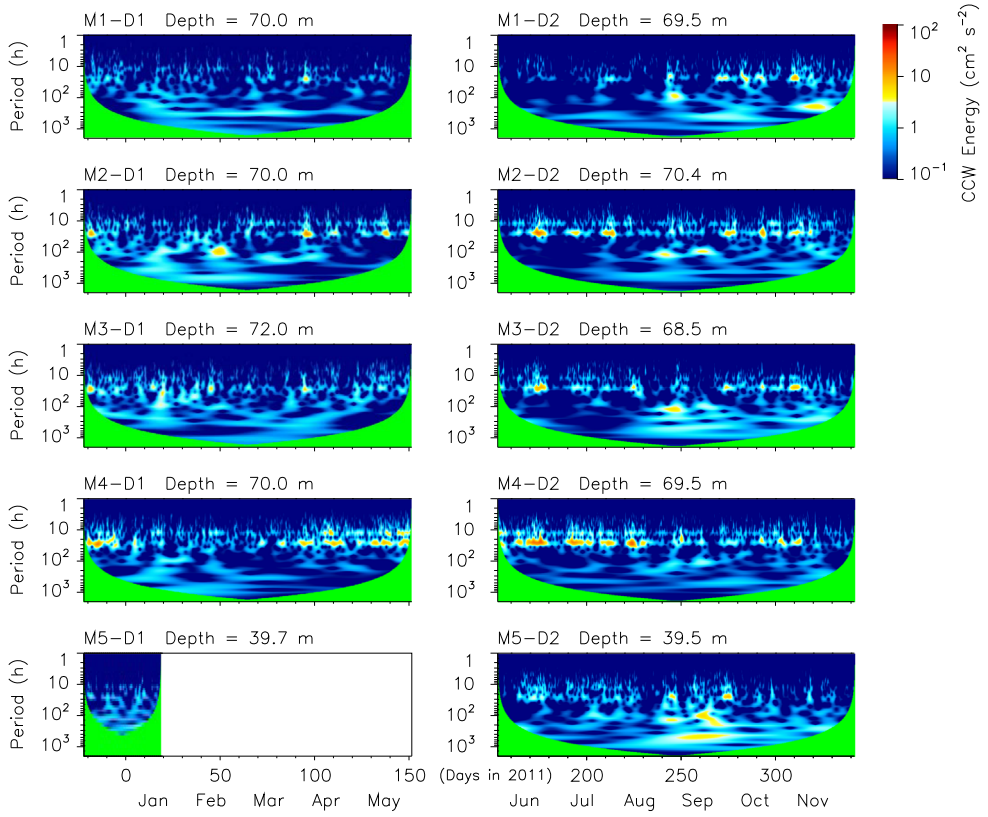

Fig. 8. Counterclockwise (CCW) energy for currents near depth=70 m (M1–M4) and 40 m (M5), as functions of period and time. Green areas indicate truncation limits, most evident for longer periods. (For interpretation of the references to color in this figure legend, the reader is referred to the web version of this article.)

M3. These LF motions are likely associated with passing eddies, as suggested during these time periods by Teague et al. (2013). CW energies near 70 m (M1–M4) and 40 m (M5) (Fig. 7) are quite similar to the shallower case (Fig. 5), but show some attenuation of the DIB levels. Much of the ~17-day energy apparent at 20 m is gone at 70 m, but at M1 there is a significant burst of several-day energy near day 245 which also corresponds to the wind burst at the end of summer. Deeper CCW energies (Fig. 8) also show reduction in DIB intensity, but not as much as for the shallower level. Note the significant deep CCW DIB energy bursts at M2 and particularly M3 near day 245; these may be related to bathymetric effects of the EFGB.

6. Wind forcing

Wavelet analysis also was applied to the wind velocities. Period–time plots of CW and CCW (S_w) appear in Fig. 9. Seasonal changes in the energy are evident with broadband frontal passages, primarily from late fall to early spring. Emergence and intensification of diurnal energy, mostly CW, are found during late spring and summer into late fall. Between days 170 and 270, the peak in energy for the DIB is well defined and is indicative of the strong sea breeze. Strong broadband summer events occur near days 170 and 210. There is some CW energy in the semidiurnal band during summer; it may be present at other times but is obscured by frontal passages and storms. We investigate possible wind forcing of the observed NICs with a wavelet coherence algorithm (Grinsted et al., 2004; Torrence and Compo, 1998). The cross-wavelet transform (C_{VVw}) for northward wind and current (at ~20 m) is defined by

$$C_{VVw} = \tilde{V}\tilde{V}_w^*, \tag{4}$$

where the asterisk denotes complex conjugate. To properly calculate coherence (γ_{VVw}), smoothing over time and frequency (Grinsted et al., 2004), indicated by an overbar, is applied to C, $\left|\tilde{V}\right|^2$, and $\left|\tilde{V}_w\right|^2$, and

$$\gamma^2{}_{VVw}(f,t) = \frac{\left|\overline{C}_{VVw}(f,t)\right|^2}{|\tilde{V}(f,t)|^2\,\overline{|\tilde{V}_w(f,t)|^2}}. \tag{5}$$

The phase of the current relative to wind fluctuations is given by

$$\phi_{VVw}(f,t) = \tan^{-1}\overline{C}_{VVw}(f,t), \tag{6}$$

Coherences of noise series (using a Monte Carlo Method) yield a 5% significance level, $\gamma_5(f)$ (only 5% of coherences with random data rise above this level). This provides a measure of confidence

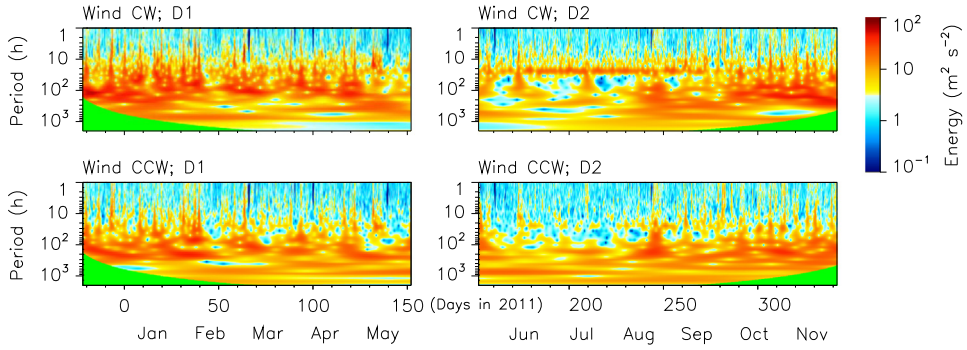

Fig. 9. CW and CCW wavelet wind energies. The time series was split to match the time intervals of the two ADCP deployments. Green areas indicate truncation limits, most evident for longer periods. (For interpretation of the references to color in this figure legend, the reader is referred to the web version of this article.)

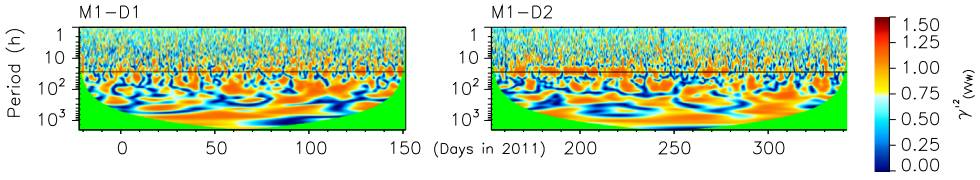

Fig. 10. Coherence-squared between ~20 m northward current and northward wind at M1. The 5% significance level is about 0.85 for periods between 2 h and about 50 days, increasing gradually for longer periods. Green areas indicate truncation limits, most evident for longer periods. 24-h period is indicated by the black line. (For interpretation of the references to color in this figure legend, the reader is referred to the web version of this article.)

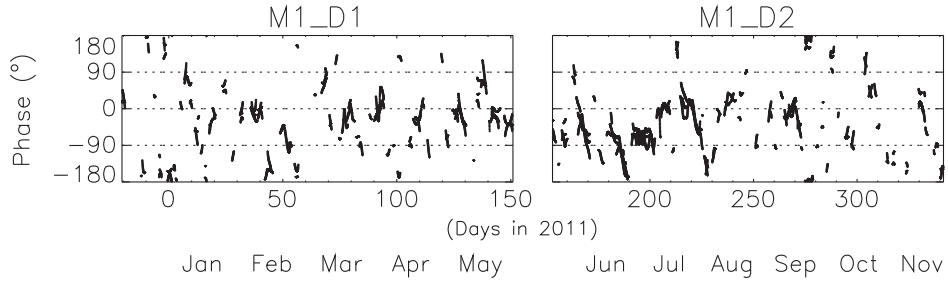

Fig. 11. Temporal phase of ~20 m northward current relative to northward wind at M1, for 3 adjacent diurnal–inertial-band periods 19.656 h, 23.375 h, 27.798 h; positive phase indicates current leading wind.

for γ_{VVw}. γ_5 is a function of frequency and ranges from 0.84 to 0.86 between periods of 1.5 h and 40 days, For longer periods it increases nearly linearly, exceeding 0.90 at 60 days. γ_5 rises sharply for periods less than 1.5 h.

Fig. 10 shows γ^2_{VVw} at M1; the other locations are qualitatively similar, as are plots of γ^2_{UUw} (not shown). The northward component was selected here to align with the principal direction (onshore–offshore) of the diurnal sea breeze, which is an important forcing agent. The similarities among locations should not be surprising since correlations among 20 m current velocities from the moorings are quite high. Significant coherences (orange to red to brown) are most evident in the diurnal–inertial range and at several-day to several-week periods. The latter correspond to energetic meridional wind events, e.g. near day 250 (see Figs. 9, 3b). Phases (Φ_{VVw}) for the 3 periods included in the DIB (Fig. 11), plotted only where γ_{VVw} is significant, show periods of reinforcing or resonance ($-90^\circ < \Phi < 90^\circ$), particularly between days 120 and 270. There are also a few short periods consistent with attenuation ($|\Phi| > 90^\circ$), e.g. near day 230.

7. Diurnal–inertial band

Zhang et al. (2009) define the band between periods of 20 h and 28 h as the diurnal inertial band (DIB). In this analysis, the wavelet band central periods (in hours) include the following: [..., 16.5290, 19.6560, 23.3750, 27.7980, 33.0570,...] (out of a total of 53 bands), so we define our DIB as the 2nd–4th of the 5 periods shown. Hence, we sum currents for these three bands to form DIB velocity

$$U_D(z,t) \equiv \sum_{k=18}^{20} \tilde{U}(z,t,f_k); \tag{7}$$

likewise for V_D and corresponding rotary components. It is useful to examine some time-dependent statistics of the DIB velocities. In the following, the statistics are 50%-overlapping two-day boxcar averages of respective quantities, yielding daily values. The time-smoothed quantities are denoted by overbars.

The smoothed energies, $\overline{S}_D$, $\overline{S}_D^+$, $\overline{S}_D^-$, can be interpreted as time and depth dependent spectra for the DIB. The CW spectral series,$\overline{S}_D^-(z,t)$, is shown in Fig. 12. The signature of $\overline{S}_D^-$ is nearly the same as that of $\overline{S}_D$ (not shown), indicating that CW energy dominates. The CCW spectra, $\overline{S}_D^+(z,t)$ (Fig. 13), show a much lower energy throughout most of the record. Notable exceptions include bursts near 70 m and day 170 at M2 and M3, and between day 140 and 230 at M4. There are other CCW bursts of shorter extent in time and depth. Where the CCW and CW energy are comparable, the currents are approximately rectilinear. The highest CW energy levels (Fig. 12) occur primarily during the spring and summer (days 110–240), but there are other, more isolated, bursts outside this.

In general, the current vectors of band-limited rotary motions describe ellipses. These ellipses can range from circular to rectilinear in shape with either CCW or CW rotation. Parameters of the ellipses, which here are functions of depth and time, can be derived from the spectra and other statistical series. The semi-major and semi-minor axes are given by

$$X_{maj} = \sqrt{\overline{S}_D^+} + \sqrt{\overline{S}_D^-}, \tag{8}$$

$$X_{\min} = \sqrt{\overline{S}_D^+} - \sqrt{\overline{S}_D^-}.$$

A positive X_{min} indicates CCW rotation; $X_{min}=0$ results if the motion is rectilinear. If $X_{min}= \pm X_{maj}$ the motion is circular. When the magnitude of the ratio $R=X_{min}/X_{maj}$ is significantly less than

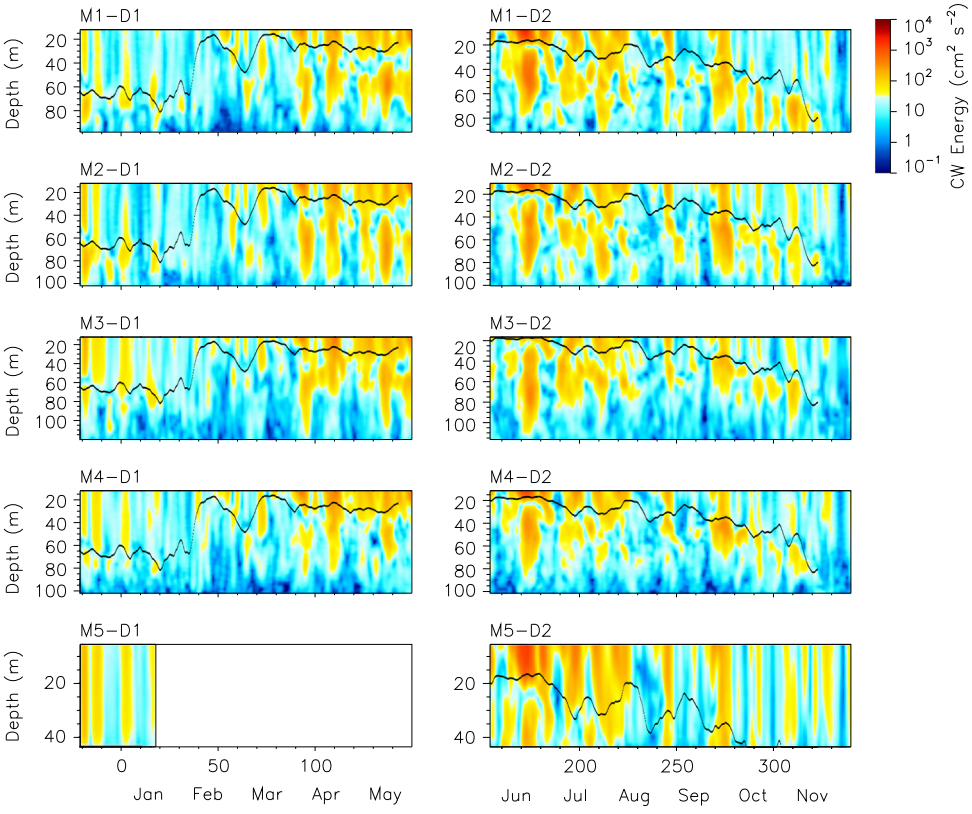

Fig. 12. Clockwise (CW) spectra for diurnal–inertial-band (DIB) currents as functions of depth and time. Statistics averaged over 2-day segments. The black curve represents mixed-layer depth.

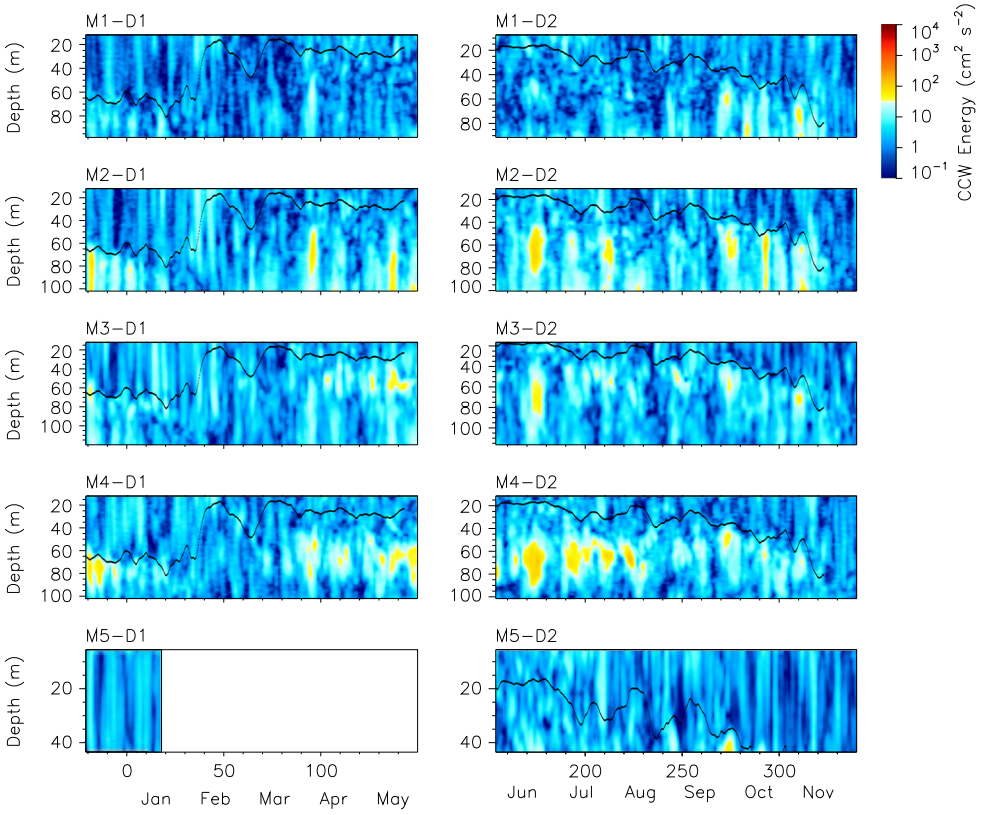

Fig. 13. Counterclockwise (CCW) spectra for diurnal–inertial-band (DIB) currents as functions of depth and time. Statistics averaged over 2-day segments. The black curve represents mixed-layer depth.

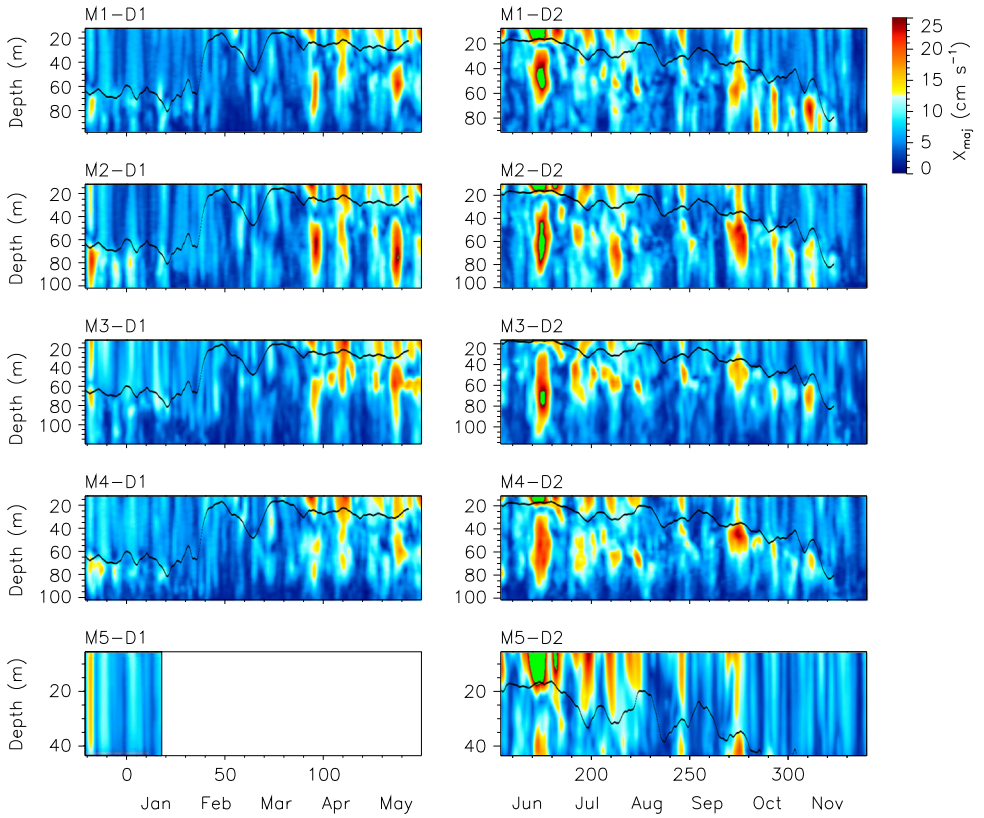

Fig. 14. Semi-major axis length for DIB current ellipses. Green areas indicate values in excess of 25 cm s^{-1}. The black curve represents mixed-layer depth. (For interpretation of the references to color in this figure legend, the reader is referred to the web version of this article.)

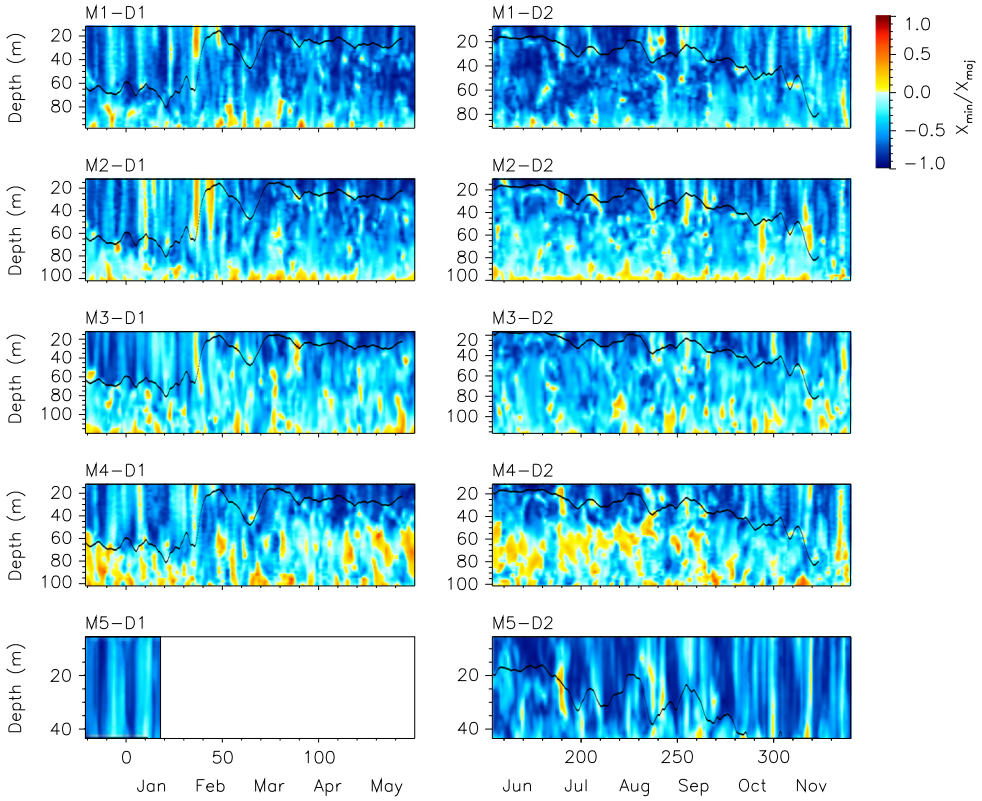

Fig. 15. Ratio of minor to major axis for DIB current ellipses. Negative values indicate clockwise rotation of the current vector. The black curve represents mixed-layer depth.

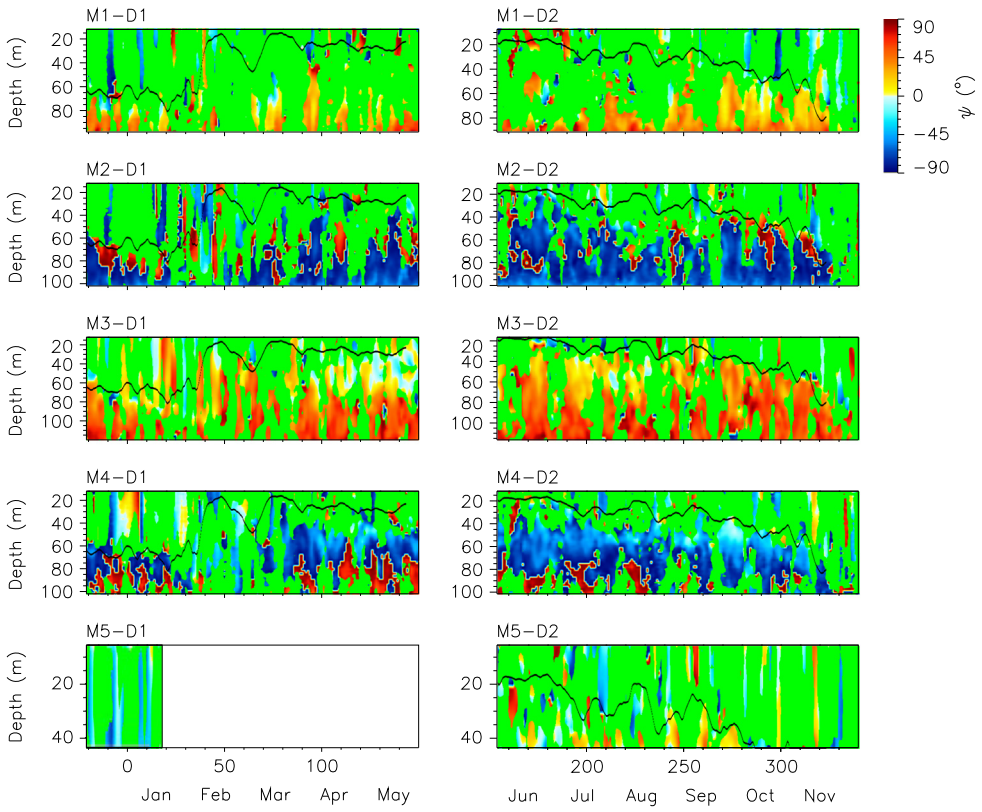

Fig. 16. Orientations of DIB current ellipses. Positive values are counterclockwise from east–west. Green areas indicate orientations that are indeterminate due to uncertainties. The black curve represents mixed-layer depth. (For interpretation of the references to color in this figure legend, the reader is referred to the web version of this article.)

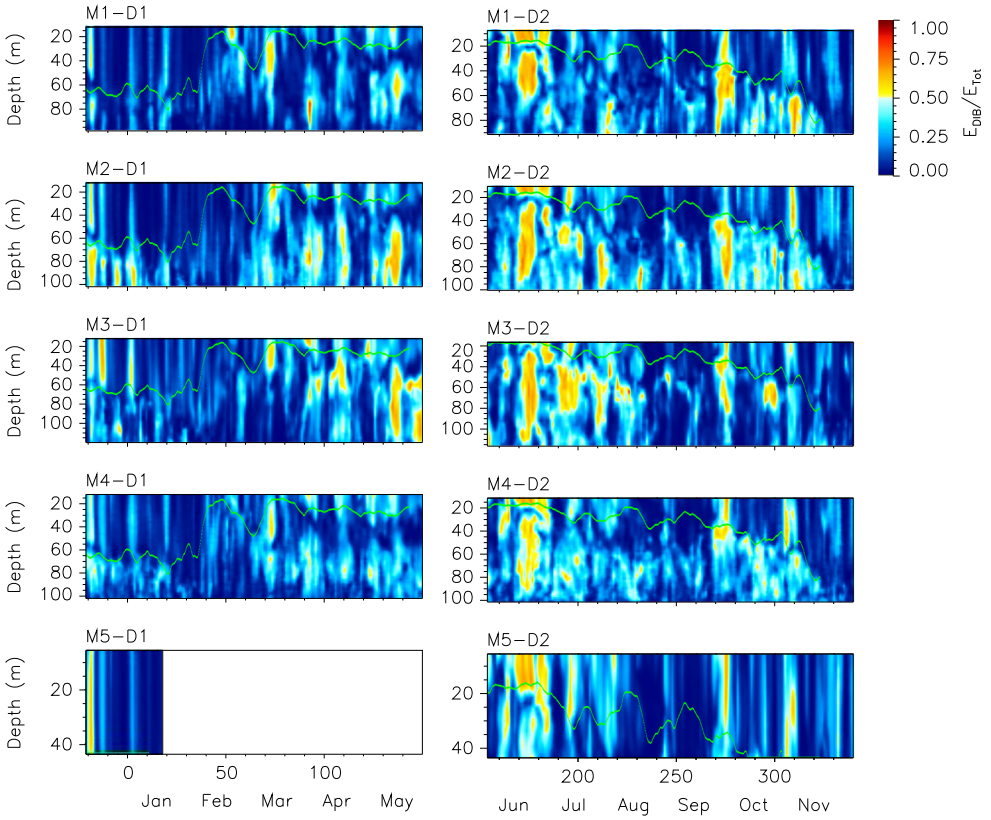

Fig. 17. Ratio of DIB energy to total energy. The green curve represents mixed-layer depth. (For interpretation of the references to color in this figure legend, the reader is referred to the web version of this article.)

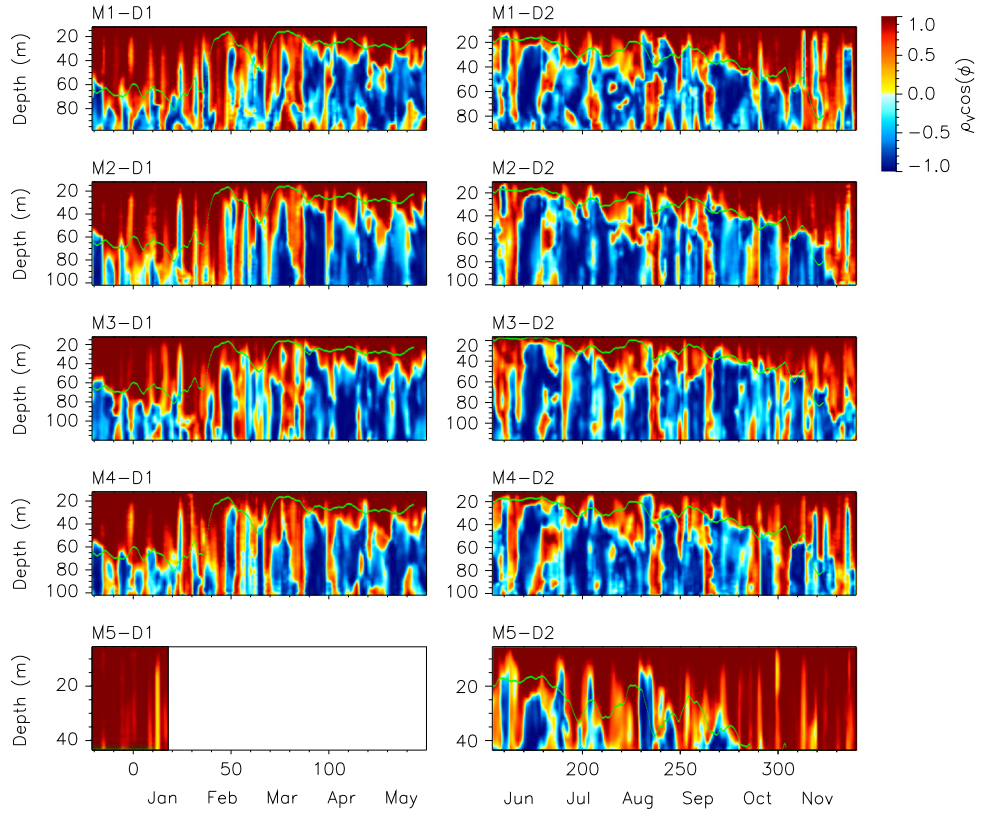

Fig. 18. DIB zero-lag correlation for $V_D(z,t)$ relative to $V_D(z_0,t)$, where z_0 is the depth of the shallowest bin. The green curve represents mixed-layer depth.

unity, it is useful to calculate ellipse orientation

$$\psi = \tan^{-1}\left(\frac{2\overline{U_D V_D}}{\overline{U_D^2} - \overline{V_D^2}}\right). \quad (9)$$

Uncertainty in ψ increases as R approaches ± 1. X_{maj} (plotted in Fig. 14) represents the smoothed DIB current amplitude; the information here is similar to that shown in Fig. 12, but is more directly comparable to current velocity. The ellipse axis ratios (R) (Fig. 15) show the dominance of CW motions in the DIB and emphasize the CCW periods, especially at M4 deeper than the top of the EFGB. The occurrences of CCW energy at M4, which was located near the steep northeast side of the EFGB, may be associated with the generation of cyclonic vortices in the lee of the bank when mean currents are eastward (Jarosz et al., submitted for publication). These CCW periods in DIB energy roughly coincide with periods of eastward mean flow reported by Teague et al. (2013; their Fig. 8a). At all locations, lighter colors (smaller magnitude of the ratio) indicate flatter ellipses, or more rectilinear fluctuations. These features suggest bathymetric effects on the flow. Ellipse orientations (or principal directions of variability) appear in Fig. 16. Much of the plot shows green areas; these are where the ratio $|R| \sim 1$ and the uncertainty in calculated ψ is greater than about 30°, rendering it meaningless. At locations where useable orientations exist (deeper than about 60 m), they are about 30°–45° at M1 and M3 and $-45°$ to $-80°$ at M2 and M4; these values align roughly with the bathymetry of the EFGB at these depths.

We can examine the ratio of energy in the DIB relative to total energy,

$$R_E(z,t) \equiv \frac{\overline{S_D}}{\overline{U^2} + \overline{V^2}} \quad (10)$$

where the overbar, as above, represents a 2-day, overlapping time average. R_E plotted in Fig. 17 is generally highest during spring–summer, with the most pronounced event occurring between days 160 and 180. The DIB energy often exceeded 50% of the total current energy and sometimes even exceeded 70% of the total energy. These high energy contributions often extended from near surface to near bottom.

Complex correlations (recall that U_D and V_D are complex series) calculated (over each 2-day segment, as above) between velocities at each depth relative to the shallowest depth yield series of magnitudes (ρ) and phases (Φ). The product $\rho \cos(\Phi)$ yields zero-lag values for U_D and V_D. The zero-lag correlation for V_D is shown in Fig. 18; the zero-lag correlation for U_D is quite similar with the main differences occurring where U values are lower, particularly at M4 below the depth of the top of the EFGB. The correlations are concentrated near 1 or -1, suggesting first-mode baroclinic motion. Also, estimates of mixed-layer depths (indicated on Fig. 18) correspond roughly to the transition from positive to negative correlations. Phases (Φ) are shown in Fig. 19. Since these results are quite noisy, the phases are assigned quadrants to provide estimates of gross changes over depth and time. In phase (315°–45°), leading (45°–135°), opposite phase (135°–225°) and lagging (225°–315°) are represented by yellow, red, green, blue, respectively. Above the mixed-layer depth the current is roughly in phase with that at the shallowest depth. Below this, the current is primarily oppositely directed. There are periods of leading and lagging fluctuations suggesting upward and downward phase propagation (or downward and upward energy propagation), respectively, but overall, the vertical structure of DIB variability suggests a first baroclinic mode. Phases and hence zero-lag correlations are questionable where DIB amplitudes are low. The deep fingers near (e.g.) days 235 and 265 at M4–D2 (Fig. 18)

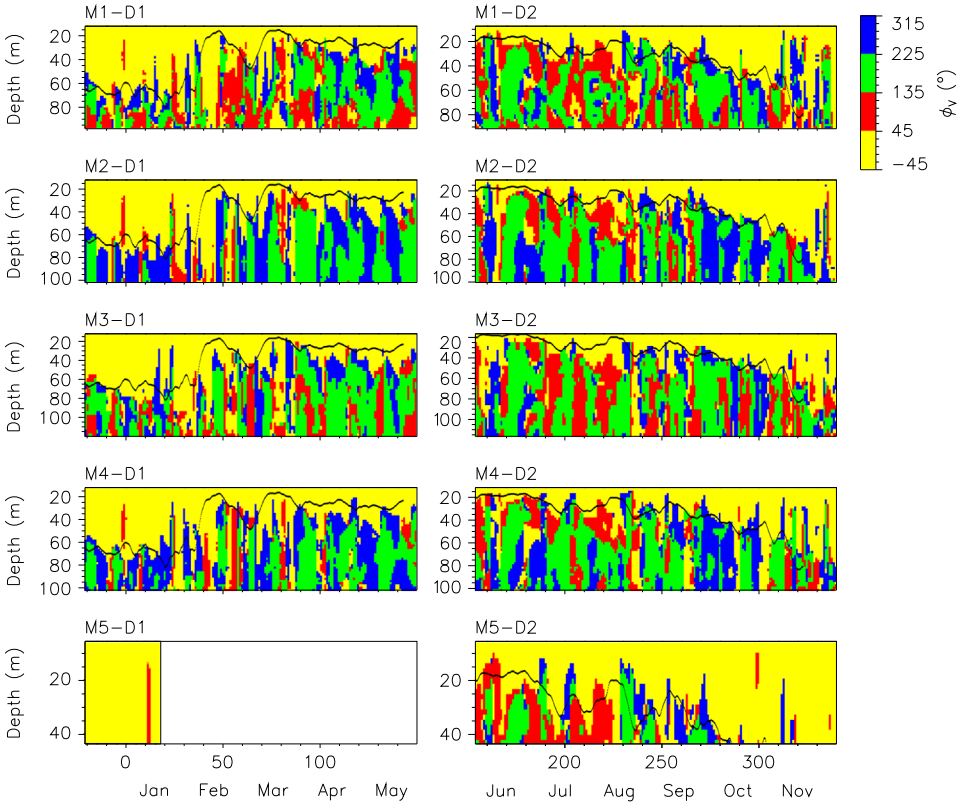

Fig. 19. Lagged correlation phase (Φ) for $V_D(z,t)$ relative to $V_D(z_0,t)$, where z_0 is the depth of the shallowest bin. Phases are expressed in quadrants centered on 0°, 90°, 180° and 270°. The black curve represents mixed-layer depth. Currents are in roughly in phase for the $-45°$–45° interval (yellow), have upward propagating phase for the 45°–135° interval (red), have opposite phase for the 135°–225° interval (green), and have downward propagating phase for the 225°–315° interval (blue). (For interpretation of the references to color in this figure legend, the reader is referred to the web version of this article.)

correspond to velocity amplitudes of about 5 cm s^{-1} or less and are primarily due to uncertainties in phase.

8. Discussion

Near-inertial currents are an important energy exchange mechanism between the winds and ocean and can be responsible for a substantial fraction of the kinetic energy throughout the water column. Our findings in the preceding sections, as well as the high horizontal coherence of currents above the bathymetry (Section 2), imply that NICs in the vicinity of the EFGB are primarily forced by winds acting on the mixed layer. Fluctuations at or near the inertial period (here, about 25.5 h) result from broadband excitation due to storms and frontal passages (Chen and Xie, 1997), while near-resonant diurnal (24 h) responses often occur when a significant sea breeze is present, mainly during late spring and summer months (DiMarco et al., 2000; Jarosz et al., 2007; Simpson et al., 2002, Rippeth et al., 2001). Furthermore, the response to wind forcing is enhanced when the mixed layer is shallow and stratification is stronger. DIB energy is input to the mixed layer as primarily CW currents with nearly circular ellipses. There is some evidence here of energy generated near the surface being propagated downward and energy generated near the bottom (by bathymetric interaction) being propagated upward (Kundu, 1976; Chant, 2001; Lerczak et al., 2001). However, the dominant mechanism in this case is likely due to the presence of the east–west boundary at the coast. This boundary allows a meridional pressure gradient to develop, associated with the north–south component of the NIC, which results in an oppositely-directed current below the pycnocline yielding a first baroclinic modal structure (Rippeth et al., 2001; Millot and Crepon, 1981; Pettigrew, 1981; Kundu et al., 1983; Tintore et al., 1995; Chen et al., 1996).

DIB energy penetrates most of the water column rather quickly (within about 1 day). Above the top of the EFGB the NIC current vectors rotate CW and their ellipses are nearly circular. Below the mixed layer the velocities become anticorrelated with the mixed-layer velocities. The ellipses flatten as depths increase beyond about 50 m with their major axes aligning roughly with the nearby bathymetry, implying significant interaction with the bank. The interaction can cause the flow to become rectilinear. In some cases (mostly at M4) the ellipses exhibit the opposite vector rotation (CCW) for extended periods; this occurs primarily when mean flow (see Fig. 8a in Teague et al., 2013) is eastward over much of the water column at M1 and M2, during spring and summer, when DIB energy is highest. The lee side of the EFGB is very steep while the west side slope is much less extreme. The eastward flow does not extend as deep at M3 and M4 due to the blocking effect of the EFGB. However, the presence of the bank in the eastward flow can produce cyclonic vortices (Jarosz et al., submitted for publication) on the lee side of the bank which may further interact with the NICs resulting in the CCW rotations seen at M4.

9. Conclusions

NICs at the EFGB occur in bursts throughout the year but are most concentrated during the spring and summer periods where they are enhanced by near-resonant sea-breeze effects. The bank tends to modify NIC characteristics below the top of the bank. NICs can occasionally reverse the predominantly eastward mean flow on short time scales. Typically, the vertical structure of the NICs followed a first-baroclinic mode with a 180° phase shift between upper and lower layers but was more complicated when waters were weakly stratified. NICs were generally stronger at the surface but sometimes were largest at mid-depth. Barotropic tidal currents were small and generally less than the NICs. Above the bank, NICs were highly coherent. Below the top of the bank, the NIC ellipses tended to align with the bathymetry and become more rectilinear while flowing around the bank. CCW rotation of the ellipse vector was common on the lee or eastern side of the bank below the top. NICs were often a significant part of the total current and could account for more than 50% of the total current energy throughout the water column. NICs are likely to be partially responsible for enhanced mixing of physical, biological, and geological properties.

The Flower Garden Banks are very important to the ecosystem in the Gulf of Mexico. Characteristics of the near-inertial currents observed at the EFGB are expected to be similar at the other banks. In combination with the mean currents and passing eddies, in the vicinity of the banks, NICs probably play a significant role in the transport and mixing of physical and biochemical properties around the numerous banks at levels significantly greater than over most of the continental shelf. Hence, they may have a pronounced effect on the ecosystem of the Gulf of Mexico shelf region. In particular, NICs are most intense during spring and summer, the period of most active biological activity, such as the mass coral spawning event that happens annually 7–10 days after the full moon, typically in the month of August.

Acknowledgments

This work was sponsored by the Bureau of Ocean Energy Management (BOEM; formerly Minerals Management Service) in the project referred to as “Currents Over Banks (COB)” through Interagency Agreement No. M10PG00038 and by the Office of Naval Research in a Naval Research Laboratory (NRL) project referred to as “Mixing Over Rough Topography (MORT)” under program element 0601153N. The measurements were made in cooperation with the Flower Garden Banks National Marine Sanctuary (administered by the National Oceanic and Atmospheric Administration (NOAA)).

References

Brooks, D.A., 1983. The wake of Hurricane Allen in the western Gulf of Mexico. J. Phys. Oceanogr. 13, 117–129.
Chant, R.J., 2001. Evolution of near-inertial waves during an upwelling event on the New Jersey inner shelf. J. Phys. Oceanogr. 31, 746–764.
Chen, C., Reid, R.O., Nowlin Jr., W.D., 1996. Near-inertial oscillations over the Texas–Louisiana shelf. J. Geophys. Res. 101, 3509–3524.
Chen, C., Xie, L., 1997. A numerical study of wind-induced, near-inertial oscillations over the Texas–Louisiana shelf. J. Geophys. Res. 102 (C7), 15583–15593, http://dx.doi.org/10.1029/97JC00228.
Daddido, E., Wiseman, W.J., Murray, S.P., 1978. Inertial currents over the inner shelf near 30 N. J. Phys. Oceanogr. 8, 728–733.
deVelasco, G.G., Winant, C.D., 1996. Seasonal patterns of wind stress and wind stress curl over the Gulf of Mexico. J. Geophys. Res. 101 (C8), 18127–18140, http://dx.doi.org/10.1029/96JC01442.
DiMarco, S.F., Reid, R.O., 1998. Characterization of the principal tidal current constituents on the Texas–Louisiana shelf. J. Geophys. Res. 103, 3093–3109.
DiMarco, S.F., Howard, M.K., Reid, R.O., 2000. Seasonal variation of wind-driven current cycling on the Texas–Louisiana continental shelf. Geophys. Res. Lett. 27 (7), 1017–1020.
Halper, F.B., McGrail, D.W., Merrell Jr., W.J., 1988. Seasonal variability in the currents on the outer Texas–Louisiana shelf. Estuar., Coast. Shelf Sci. 26, 33–50.
Gonella, J., 1972. A rotary-component method for analyzing meteorological and oceanographic vector time series. Deep Sea Res. 19, 833–846.
Grinsted, A., Moore, J.C., Jevrejeva, S., 2004. Application of the cross wavelet transform and wavelet coherence to geophysical time series. Nonlinear Process. Geophys. 11, 561–566, http://dx.doi.org/10.5194/npg-11-561-2004.
Jarosz, E., Hallock, Z.R., Teague, W.J., 2007. Near-inertial currents in the DeSoto Canyon region. Cont. Shelf Res. 27, 2407–2426.
Jarosz, E., Wijesekera, H.W., Teague, W.J., Fribance, D.B., Moline, M.A., 2014. Observations on stratified flow over a bank at low Froude numbers. J. Geophys. Res. (submitted for publication).

Kundu, P.K., 1976. An analysis of inertial oscillations observed near the Oregon coast. J. Phys. Oceanogr. 6, 879–893.
Kundu, P.K., Chao, S.-Y., McCreary, J.P., 1983. Transient coastal currents and inertio-gravity waves. Deep-Sea Res. 30, 1059–1082.
Lerczak, J.A., Hendershott, M.C., Winant, C.D., 2001. Observations and modeling of coastal internal waves driven by a diurnal sea breeze. J. Geophys. Res. 106, 19,715–19,729.
Liu, P.C., Miller, G.S., 1996. Wavelet Transforms and Ocean Current Data Analysis. J. Atmos. Ocean. Technol. 13, 1090–1099.
Mallat, S.G., 1989. A theory for multiresolution signal decomposition: the wavelet representation. IEEE Trans. Pattern Anal. Mach. Intell. 11 (7), 674–693.
McGrail, D.W., 1983. Flow, boundary layers, and suspended sediment at the Flower Garden Banks. In: Rezak, R., Bright, T.J., McGrail, D.W. (Eds.), Reefs and Banks of the Northwestern Gulf of Mexico: Their Geological, Biological, and Physical Dynamics. Final Report, Technical Report no. 83-1-T. U.S. Department of the Interior, Minerals Management Service, Gulf of Mexico OCS Regional Office, New Orleans, LA, pp. 141–230.
Millot, C., Crépon, M., 1981. Inertial oscillations on the continental shelf of the Gulf of Lions – observations and theory. J. Phys. Oceanogr. 11, 639–657.
Mooers, C.N.K., 1973. A technique for the cross spectrum analysis of pairs of complex-valued time series, with emphasis on properties of polarized components and rotational invariants. Deep-Sea Res. Oceanogr. Abstracts 20 (12), 1129–1141.
Moum, J.N., Nash, J.D., 2000. Topographically induced drag and mixing at a small bank on the continental shelf. J. Phys. Oceanogr. 30, 2049–2054.
Perkins, H., 1972. Inertial oscillations in the Mediterranean. Deep-Sea Res. 19, 289–296.
Perkins, H., De Strobel, F., Gauldesi, L., 2000. The Barny sentinal trawl-resistant ADCP bottom mount: design, testing, and application. IEEE J. Ocean. Eng. 25, 430–436.
Pettigrew, N.R., 1981. The dynamics and kinematics of the coastal boundary layer off Long Island. Ph.D. thesis, Massachusetts Institute of Technology/Woods Hole Oceanographic Institution, WHOI-81-14, 262 p.
Pollard, R.T., 1970. On the generation by winds of inertial waves in the ocean. Deep-Sea Res. 17, 795–812.
Price, J.F., 1976. Several aspects of the response of shelf waters to a cold front passage. Mem. Soc. Sci. Liege 6e series X, 201–208.
Rippeth, T.P., Simpson, J.H., Player, R.J., Garcia, M., 2001. Current oscillations in the diurnal–inertial band on the Catalonian Shelf in spring. Continental Shelf Res. 22 (2), 247–265.
Simpson, J.H., Hyder, P., Rippeth, T.P., Lucas, I.M., 2002. Forced oscillations near the critical latitude for diurnal–inertial resonance. J. Phys. Oceanogr. 32, 177–187.
Teague, W.J., Jarosz, E., Wang, D.W., Mitchell, D.A., 2007. Observed oceanic response over the upper continental slope and outer shelf during Hurricane Ivan. J. Phys. Oceanogr. 37, 2181–2206.
Teague, W.J., Wijesekera, H.W., Jarosz, E., Fribance, D.B., Lugo-Fernandez, A., Hallock, Z.R., 2013. Current and hydrographic conditions at the East Flower Garden Bank in 2011. Cont. Shelf Res. 63, 43–58.
Tintore, J., Wang, D.-P., Garcia, E., Viudez, A., 1995. Near-inertial motions in the coastal ocean. J. Mar. Syst. 6, 301–312.
Torrence, C., Compo, G.P., 1998. A practical guide to wavelet analysis. Bull. Am. Meteorol. Soc. 79, 61–78.
Webster, F., 1968. Observations of inertial-period motions in the deep sea. Rev. Geophys. 6, 473–490.
Zhang, X., DiMarco, S.F., Smith IV, D.C., Howard, M.K., Jochens, A.E., Hetland, R.D., 2009. Near-resonant ocean response to sea breeze on a stratified continental shelf. J. Phys. Oceanogr. 39, 2137–2155.